Supporting Information: The key role of non-local screening in the environment-insensitive exciton fine structures of transition-metal dichalcogenide monolayers

Wei-Hua Li,[†] Jhen-Dong Lin,[†] Ping-Yuan Lo,[†] Guan-Hao Peng,[†] Ching-Yu Hei,[†] Shao-Yu Chen,[‡] and Shun-Jen Cheng*[,†]

†*Department of Electrophysics, National Yang Ming Chiao Tung University, Hsinchu 300, Taiwan*

‡*Center of Condensed Matter Sciences, National Taiwan University, Taipei 106, Taiwan*

¶*Center of Atomic Initiative for New Material, National Taiwan University, Taipei 106, Taiwan*

E-mail: sjcheng@nycu.edu.tw

Non-local dielectric function of layered structure

The matrix elements of the electron-hole (e-h) direct Coulomb interaction in the Bethe-Salpeter equation (BSE) represent the amplitudes of the Coulomb scattering between the charge pair densities via the screened Coulomb interaction. The screened Coulomb interaction is essentially the Green's function that describes the interaction between two point charges. With the dielectric screening of media, the screened Coulomb interaction W at $\boldsymbol{r}_1$

with a point charge located $\boldsymbol{r}_2$ obeys the Poisson's equation[1–4]

$$\nabla_{\boldsymbol{r}_1} \cdot \int d^3\boldsymbol{r}' \, \varepsilon(\boldsymbol{r}_1, \boldsymbol{r}') \nabla_{\boldsymbol{r}'} W(\boldsymbol{r}', \boldsymbol{r}_2) = -\frac{e^2}{\varepsilon_0} \delta(\boldsymbol{r}_1 - \boldsymbol{r}_2), \tag{S1}$$

where $\varepsilon(\boldsymbol{r}_1, \boldsymbol{r}')$ is the dielectric function. Due to the lattice translational symmetries of the screened Coulomb interaction and the dielectric function in 2D plane, we can expand the screened Coulomb interaction and the dielectric function by the in-plane Fourier series which is defined as

$$f_{\boldsymbol{G}_1\boldsymbol{G}_2}(\boldsymbol{q}; z_1, z_2) = \frac{1}{\mathcal{A}} \int d^2\boldsymbol{\rho}_1 d^2\boldsymbol{\rho}_2 \, e^{-i(\boldsymbol{q}+\boldsymbol{G}_1)\cdot\boldsymbol{\rho}_1} f(\boldsymbol{\rho}_1, z_1, \boldsymbol{\rho}_2, z_2) e^{i(\boldsymbol{q}+\boldsymbol{G}_2)\cdot\boldsymbol{\rho}_2}, \tag{S2}$$

where $\boldsymbol{G}$ is the reciprocal lattice vector and $\boldsymbol{\rho} = (x, y)$ is the in-plane coordinate. By using the Fourier series, the Poisson's equation is reformulated as

$$\sum_{\boldsymbol{G}'} \int dz' \left[-(\boldsymbol{q}+\boldsymbol{G}_1)\cdot(\boldsymbol{q}+\boldsymbol{G}')\varepsilon_{\boldsymbol{G}_1\boldsymbol{G}'}(\boldsymbol{q}; z_1, z') + \frac{\partial}{\partial z_1}\varepsilon_{\boldsymbol{G}_1\boldsymbol{G}'}(\boldsymbol{q}; z_1, z')\frac{\partial}{\partial z'}\right] W_{\boldsymbol{G}'\boldsymbol{G}_2}(\boldsymbol{q}; z', z_2)$$
$$= -\frac{e^2}{\varepsilon_0}\delta_{\boldsymbol{G}_1\boldsymbol{G}_2}\delta(z_1 - z_2). \tag{S3}$$

Since the *e*-*h* direct Coulomb interaction is dominated by the long-range component,[1,5,6] we take the long-range approximation ($\boldsymbol{G}_1 = \boldsymbol{G}_2 = \boldsymbol{G}' = \boldsymbol{0}$) for the Poisson's equation Eq. (S3), and assume that the dielectric function is local in z-direction,[1–3]

$$\varepsilon_{\boldsymbol{00}}(\boldsymbol{q}; z_1, z') \approx \varepsilon_{\boldsymbol{00}}(\boldsymbol{q}; z_1)\delta(z_1 - z') \, . \tag{S4}$$

For simplification of the notations, hereafter we omit the indices of reciprocal lattice vector $\boldsymbol{G}$, and the notations are changed as $\varepsilon_{\boldsymbol{q}}(z_1) = \varepsilon_{\boldsymbol{00}}(\boldsymbol{q}; z_1)$ and $W(\boldsymbol{q}; z_1, z_2) = W_{\boldsymbol{00}}(\boldsymbol{q}; z_1, z_2)$. Accordingly, the screened Coulomb interaction in the momentum space can be obtained by

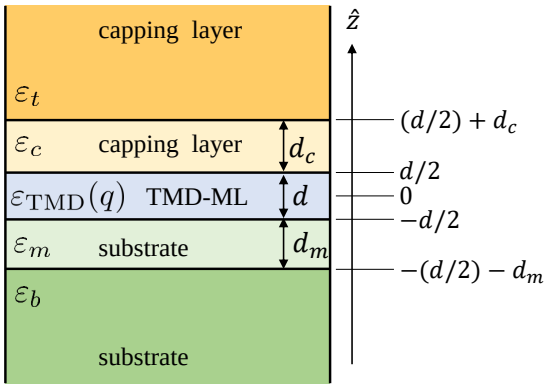

Figure S1: The schematics of the five-layer structure with TMD embedded in the middle, which gives rise to the piece-wise dielectric function of Eq. (S6). The q-dependent bulk dielectric function of TMD, $\varepsilon_{\mathrm{TMD}}(q)$, is adopted for the layer of TMD-ML. ε_b, ε_m, ε_c and ε_t are the dielectric constants of the environmental media. d_m and d_c are the thicknesses of the middle substrate and the middle capping layer, respectively.

solving the Poisson equation

$$\left[-q^2\varepsilon_{\boldsymbol{q}}(z_1)+\frac{\partial}{\partial z_1}\varepsilon_{\boldsymbol{q}}(z_1)\frac{\partial}{\partial z_1}\right]W(\boldsymbol{q};z_1,z_2)=-\frac{e^2}{\varepsilon_0}\delta(z_1-z_2). \tag{S5}$$

Following the approach of Refs.[1–3], the dielectric function is assumed to be isotropic in 2D plane and is taken as the piece-wise function in z-direction with the values depending on the positions of TMD-ML, substrates and capping layers (see Fig. S1). For the 5-layer structure, $\varepsilon_{\boldsymbol{q}}(z_1)$ is given by

$$\varepsilon_{\boldsymbol{q}}(z_1)=\begin{cases}\varepsilon_t, & z_1>\frac{d}{2}+d_c\\ \varepsilon_c, & \frac{d}{2}<z_1<\frac{d}{2}+d_c\\ \varepsilon_{\mathrm{TMD}}(q), & -\frac{d}{2}<z_1<\frac{d}{2}\\ \varepsilon_m, & -\frac{d}{2}-d_m<z_1<-\frac{d}{2}\\ \varepsilon_b, & z_1<-\frac{d}{2}-d_m\end{cases} \tag{S6}$$

where $q=|\boldsymbol{q}|$, ε_t, ε_c, ε_m and ε_b are the dielectric constants of layers surrounding TMD-ML,

Table S1: Dielectric constants of environmental materials in this work.

Material	SiO_2 [9]	hBN [10,11]	Al_2O_3 [12]	HfO_x [13]
Dielectric constant	3.9	4.5	9.2	15

d is the thickness of TMD-ML layer, d_c and d_m are the thickness of the middle capping layer and middle substrate with dielectric constant ε_c and ε_m, respectively. For the layer of TMD-ML, we adopt the q-dependent dielectric function of bulk TMD in the random-phase approximation[7,8]

$$\varepsilon_{\mathrm{TMD}}(q) = 1 + \frac{1}{(\varepsilon_{2D}-1)^{-1} + \alpha\frac{q^2}{q_{TF}^2} + (\frac{\hbar^2 q^2}{2m_0 E_{pl}})^2} \tag{S7}$$

where ε_{2D} is the in-plane dielectric constant of the bulk TMD, E_{pl} is the plasma peak energy, $\alpha = 1.55$[8] is the fitting parameter and $q_{TF} = \sqrt{\frac{e^2 m_0}{\pi^2\varepsilon_0\hbar^2}(\frac{3\pi^2\varepsilon_0 m_0 E_{pl}^2}{e^2\hbar^2})^{1/3}}$ is the Thomas-Fermi wave vector.[1,8]

Based on the piece-wise dielectric function in z-direction and the vanished potential at infinities ($z \to \pm\infty$), the solution of the screened Coulomb interaction with the source charge located in the layer of TMD-ML, i.e., $-\frac{d}{2} < z_2 < \frac{d}{2}$, has the form

$$W(\boldsymbol{q}, z_1, z_2) = \frac{e^2}{2q\varepsilon_0\varepsilon_{\boldsymbol{q}}(z_1)} \begin{cases} C_1 e^{-qz_1}, & z_1 > \frac{d}{2} + d_c \\ C_2 e^{-qz_1} + C_3 e^{qz_1}, & \frac{d}{2} < z_1 < \frac{d}{2} + d_c \\ C_4 e^{-qz_1} + C_5 e^{qz_1} + e^{-q|z_1 - z_2|}, & -\frac{d}{2} < z_1 < \frac{d}{2} \\ C_6 e^{-qz_1} + C_7 e^{qz_1}, & -\frac{d}{2} - d_m < z_1 < -\frac{d}{2} \\ C_8 e^{qz_1}, & z_1 < -\frac{d}{2} - d_m \end{cases} \tag{S8}$$

The coefficients C_i can be found out by the electrostatic boundary conditions[1,14,15]

$$W(\boldsymbol{q}; z_1 = d_i^+, z_2) = W(\boldsymbol{q}; z_1 = d_i^-, z_2) \tag{S9}$$

$$\varepsilon_{\boldsymbol{q}}(z_1 = d_i^+)\ \frac{\partial}{\partial z_1} W(\boldsymbol{q}; z_1, z_2)\Big|_{z_1 = d_i^+} = \varepsilon_{\boldsymbol{q}}(z_1 = d_i^-)\ \frac{\partial}{\partial z_1} W(\boldsymbol{q}; z_1, z_2)\Big|_{z_1 = d_i^-} \tag{S10}$$

where d_i denotes the the positions of the interfaces in the z-coordinate. After deriving $W(\boldsymbol{q}; z_1, z_2)$, the effective dielectric function is defined as the ratio of the z-averaged unscreened Coulomb interaction to the screened one

$$\varepsilon(\boldsymbol{q}) = V(\boldsymbol{q})/W(\boldsymbol{q}), \tag{S11}$$

where

$$W(\boldsymbol{q}) = \frac{1}{d^2}\int_{-d/2}^{d/2}\int_{-d/2}^{d/2} dz_1 dz_2\, W(\boldsymbol{q}, z_1, z_2), \tag{S12}$$

and

$$\begin{aligned} V(\boldsymbol{q}) =& \frac{1}{d^2}\int_{-d/2}^{d/2} dz_1 \int_{-d/2}^{d/2} dz_2 \int d^2\boldsymbol{\rho}\, V(\boldsymbol{\rho}; z_1 - z_2)\, e^{-i\boldsymbol{q}\cdot\boldsymbol{\rho}} \\ =& \frac{e^2}{4\pi\varepsilon_0}\frac{4\pi}{dq^2}\left(1 - \frac{1 - e^{-qd}}{qd}\right). \end{aligned} \tag{S13}$$

The dielectric function of the 5-layer structure is given by

$$\varepsilon(\boldsymbol{q}) = \frac{\varepsilon_{\mathrm{TMD}}(q)}{D(\boldsymbol{q})} \tag{S14}$$

where

$$
\begin{aligned}
D(\boldsymbol{q}) =& 1 + \Bigg\{ \Bigg\{ e^{-2dq}(e^{dq}-1)^2 \\
&\times \Big[\sinh(d_m q) \Big(-e^{dq} \big(\sinh(d_c q)(\varepsilon_m^2 \varepsilon_c^2 - \varepsilon_{\mathrm{TMD}}^2(q)\varepsilon_b\varepsilon_t) - \varepsilon_c \cosh(d_c q)(\varepsilon_{\mathrm{TMD}}^2(q)\varepsilon_b - \varepsilon_t \varepsilon_m^2) \big) \\
&\quad + (\varepsilon_{\mathrm{TMD}}(q)\varepsilon_b - \varepsilon_m^2) \big(\sinh(d_c q)(\varepsilon_{\mathrm{TMD}}(q)\varepsilon_t - \varepsilon_c^2) \\
&\quad\quad + \cosh(d_c q)\varepsilon_c(\varepsilon_{\mathrm{TMD}}(q) - \varepsilon_t) \big) \Big) \\
&\quad + \varepsilon_m \cosh(d_m q) \Big(e^{dq} \big(\sinh(d_c q)(\varepsilon_{\mathrm{TMD}}^2(q)\varepsilon_t - \varepsilon_b \varepsilon_c^2) - \varepsilon_c \cosh(d_c q)(\varepsilon_b \varepsilon_t - \varepsilon_{\mathrm{TMD}}^2(q)) \big) \\
&\quad\quad + (\varepsilon_{\mathrm{TMD}}(q) - \varepsilon_b) \big(\sinh(d_c q)(\varepsilon_{\mathrm{TMD}}(q)\varepsilon_t - \varepsilon_c^2) \\
&\quad\quad\quad + \varepsilon_c \cosh(d_c q)(\varepsilon_{\mathrm{TMD}}(q) - \varepsilon_t) \big) \Big) \Big] \Bigg\} \\
&\times \Bigg\{ 2\sinh(dq) \Big[\sinh(d_m q) \Big(\sinh(d_c q) \big(\varepsilon_m^2 \varepsilon_c^2 + \varepsilon_{\mathrm{TMD}}^2(q)\varepsilon_b\varepsilon_t \big) + \varepsilon_c \cosh(d_c q)(\varepsilon_{\mathrm{TMD}}^2(q)\varepsilon_b + \varepsilon_t \varepsilon_m^2) \Big) \\
&\quad + \varepsilon_m \cosh(d_m q) \Big(\sinh(d_c q) \big(\varepsilon_{\mathrm{TMD}}^2(q)\varepsilon_t + \varepsilon_b \varepsilon_c^2 \big) \\
&\quad\quad + \varepsilon_c \cosh(d_c q) \big(\varepsilon_b \varepsilon_t + \varepsilon_{\mathrm{TMD}}^2(q) \big) \Big) \Big] \\
&\quad + 2\varepsilon_{\mathrm{TMD}}(q)\cosh(dq) \Big[\sinh(d_m q) \Big(\sinh(d_c q) \big(\varepsilon_t \varepsilon_m^2 + \varepsilon_b \varepsilon_c^2 \big) + \varepsilon_c \cosh(d_c q) \big(\varepsilon_b \varepsilon_t + \varepsilon_m^2 \big) \Big) \\
&\quad\quad + \varepsilon_m \cosh(d_m q) \Big(\sinh(d_c q) \big(\varepsilon_b \varepsilon_t + \varepsilon_c^2 \big) + \varepsilon_c \cosh(d_c q) \big(\varepsilon_b + \varepsilon_t \big) \Big) \Big] \Bigg\}^{-1} \\
&\times (e^{-dq} + dq - 1)^{-1} \Bigg\}. \qquad \text{(S15)}
\end{aligned}
$$

For the parameters in the bulk dielectric function $\varepsilon_{\mathrm{TMD}}(q)$ of WSe_2-ML, we adopt $\alpha = 1.55$,[8] the thickness $d = 6.72$ Å,[16] the in-plane dielectric constant $\varepsilon_{2D} = 13.8$,[17] and the plasma peak energy $E_{pl} = 22.6$ eV.[18] The used dielectric constants of capping layers and substrates in this work are listed in Table. S1.

After deriving the dielectric function and the screened Coulomb interaction of TMD-ML, the matrix elements of the *e-h* direct Coulomb interaction in the Bethe-Salpeter equation can be calculated. The methodology of calculating the matrix elements of the electron-hole Coulomb interaction are detailed in the supporting information of our previous publication

Ref.[5].

Experiment photoluminescence spectrum

The sample fabrication and photoluminescence (PL) measurement of the experiment data in Fig. S2 are described as the following. We exfoliated WSe_2 from the bulk WSe_2 crystal purchased from HQ Graphene. The WSe_2-ML flakes are firstly exfoliated on a PDMS stamp and inspected under optical microscope. The thickness of WSe_2 is confirmed by optical contrast and optical spectroscopy. Then, we transferred the flakes on the desired substrates (e.g. SiO_2, Al_2O_3, etc.) For hBN-encapsulated WSe_2-ML samples, we followed the fabrication procedures of PPC-assisted transfer mentioned in Ref.[19]. The top and bottom hBN are chosen around 20 nm to ensure good passivation and protection.

After fabrication, the samples were mounted in a Janis (ST-500) cryostat maintained at a high vacuum (5×10^{-6} torr) and cooled down to 10 K by flowing liquid helium. For PL spectroscopy, we excited the sample by a CW laser with wavelength at 532 nm. We employed a 40× objective lens (NA: 0.6) to focus the laser to a spot size of about ~ 1 μm on the sample and to collect the PL signal in back-scattering geometry. The signal was guided to the Horiba iHR 550 spectrometer and then detected by the liquid-nitrogen cooled charge-coupled device of Horiba Symphony II detection system.

Comparison of experiment photoluminescence and BSE calculation

The quasi-particle states of WSe_2-ML in DFT are carried out by utilizing the VASP [20] with the Heyd-Scuseria-Ernzhof (HSE) exchange-correlation functional.[21] We employ the experimental lattice constant 3.282 Å [22,23] in the DFT calculation. The energy cutoff of the plane-wave basis is set to be 500 eV for the expansion of the wavefunctions and the projector-

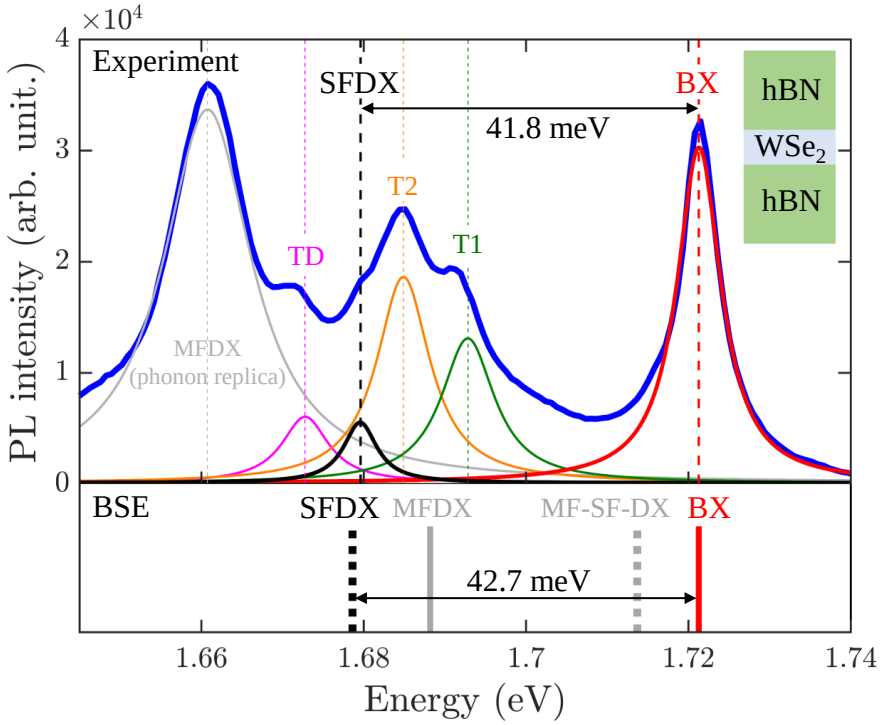

Figure S2: Comparison of the measured fine structure spectrum of PL at $T = 10$K (top panel) and BSE-calculated exciton fine structure (bottom panel) of hBN-encapsulated WSe_2-ML. In the top panel, the measured PL spectrum is indicated by the blue profile. Based on the assignments of the PL peaks in Ref.,[19] the fitted peak by the red (black) profile is attributed to the BX (SFDX) states. In the bottom panel, the vertical lines indicate the BSE-calculated energies of the BX and various DX states, in a quantitative agreement with the fine structure of the measured PL spectrum. The other fitted peaks in the PL spectrum are attributed to the states of the inter-valley negatively charged trion (T1), the intra-valley negatively charged trion (T2) and the exciton-trion five-particle state (TD).[19]

augmented wave (PAW) potentials. The gamma-centered k-grid of $9\times9\times1$ is taken to sample the Brillouin zone and the electronic relaxation convergence limit is set as 10^{-6} eV. In order to simulate the suspended WSe_2 monolayer, the distance between the periodic layers in the out-of-plane direction is set to be greater than 30 Å. The structure relaxation is performed with the convergence limit of 0.005 eV/Å.

On the base of the DFT-calculated band structure, we calculate the exciton fine structure of hBN-encapsulated WSe_2-ML and compare the BSE-calculated exciton fine structure with the experimental PL spectrum. From the PL spectrum of hBN-encapsulated WSe_2-ML shown in the top panel of Fig. S2, the energy of the bright exciton (BX) is 1.7213 eV and the

Table S2: Summary of the measured fine structure splittings between BX and SFDX states of WSe_2 monolayers embedded in different dielectric structures by the existing experiments. The superscript $*$ marks the calculated splittings by this work.

Dielectric structure	Measured $\Delta^X_{B,SF}$ (meV)	References
Air/WSe_2/SiO_2	51.2*	Our BSE calculation
Air/WSe_2/SiO_2	47	[24]
Air/WSe_2/SiO_2	47	[25]
Air/WSe_2/hBN	49.9*	Our BSE calculation
Air/WSe_2/hBN	43	[26]
hBN/WSe_2/SiO_2	43.7*	Our BSE calculation
hBN/WSe_2/SiO_2	46	[26]
hBN/WSe_2/hBN	42.7*	Our BSE calculation
hBN/WSe_2/hBN	41.8	Our experiment work
hBN/WSe_2/hBN	38	[27]
hBN/WSe_2/hBN	40	[19]
hBN/WSe_2/hBN	40	[28–30]
hBN/WSe_2/hBN	41	[31–33]
hBN/WSe_2/hBN	41	[34]
hBN/WSe_2/hBN	42	[35]
hBN/WSe_2/hBN	42	[36]
hBN/WSe_2/hBN	42	[37]
hBN/WSe_2/hBN	43	[38]
hBN/WSe_2/hBN	43	[39]
hBN/WSe_2/hBN	43	[40]
hBN/WSe_2/hBN	43	[41,42]
hBN/WSe_2/hBN	44	[26]

energy of the spin-forbidden dark exciton (SFDX) is 1.6795 eV, which shows that the energy splitting is 41.8 meV. In the bottom panel of Fig. S2, the BSE-calculated energy splitting between BX and SFDX is 42.7 meV, which is in an excellent agreement with the measured splitting.

Further, we make the comparison of the BSE-calculated and experimentally measured BX-SFDX splittings of WSe_2-ML in the dielectric structures of air/WSe_2/SiO_2, air/WSe_2/hBN, hBN/WSe_2/SiO_2 and hBN/WSe_2/hBN, as summarized by Table. S2.,[19,24–42] Basically, the BSE-calculated splittings are in fairly good agreement with the measured ones. From the data of Table. S2, one can note that the magnitudes of the fine structure splittings of WSe_2-ML in the different dielectric structures are weakly environment-dependent.

The effective dielectric constant

In the extended hydrogen model, we estimate the effective dielectric constant of S-state exciton by averaging the dielectric function in $\boldsymbol{q}$-space within the circle $|\boldsymbol{q}| \leq 2/a_S^X$ [43]

$$\varepsilon_{eff,S} \approx 2\left(\frac{a_S^X}{2}\right)^2 \int_0^{2/a_S^X} dq\; q\varepsilon(q) \tag{S16}$$

where $a_S^X = \frac{4\pi\varepsilon_0\hbar^2}{e^2}\frac{\varepsilon_{eff,S}}{\mu_S}$ is the exciton Bohr radius, and μ_S is the reduced mass of the exciton. Eq. (S16) is essentially a self-consistent equation.

For simplicity, we consider the cases of the the TMD-ML encapsulated by two semi-infinite dielectrics by employing $\varepsilon_t = \varepsilon_c = \varepsilon_m = \varepsilon_b = \varepsilon_{env}$ in the model calculations for Fig.4 of the main article. In addition, because the dielectric function of bulk TMD weakly depends on q when q is small, we approximate $\varepsilon_{\rm TMD}(q) \approx \varepsilon_{2D} = 13.8$ for WSe_2. By expanding $\varepsilon(q)$ in the Taylor series with respect to q up to the first- or second-order terms, $\varepsilon_{eff,S}$ is solvable according to Eq. (S16).

First-order approximation

In the first-order approximation, we take $\varepsilon(q) \approx c_0 + c_1 q$ and, from Eq. (S16), derive

$$\varepsilon_{eff,S} = c_0 + \frac{e^2}{3\pi\varepsilon_0\hbar^2}\frac{\mu_S}{\varepsilon_{eff,S}}c_1\,. \tag{S17}$$

Accordingly, we solve

$$\varepsilon_{eff,S} \approx \varepsilon_{eff,S}^{(1)} = \frac{c_0}{2} + \frac{1}{2}\sqrt{c_0^2 + \frac{4e^2}{3\pi\varepsilon_0\hbar^2}\mu_S c_1}\,. \tag{S18}$$

Defining $\Delta\varepsilon = \varepsilon_{eff,D} - \varepsilon_{eff,B}$, one can show

$$\Delta\varepsilon = \frac{1}{2}\sqrt{c_0^2 + \frac{4e^2c_1}{3\pi\varepsilon_0\hbar^2}\mu_D} - \frac{1}{2}\sqrt{c_0^2 + \frac{4e^2c_1}{3\pi\varepsilon_0\hbar^2}\mu_B}\,. \tag{S19}$$

in the first-order approximation for the Taylor-expanded $\varepsilon(q)$ with respect to q.

Second-order approximation

For the better quantitative evaluation of $\varepsilon_{eff,S}$, one can take the second-order approximation of $\varepsilon(q)$ to solve Eq. (S16), which gives rise to

$$\varepsilon_{eff,S} = c_0 + \frac{e^2}{3\pi\varepsilon_0\hbar^2}\frac{\mu_S}{\varepsilon_{eff,S}}c_1 + 2\left(\frac{e^2}{4\pi\varepsilon_0\hbar^2}\right)^2\frac{\mu_S^2}{\varepsilon_{eff,S}^2}c_2. \tag{S20}$$

Because the range of the integration of Eq. (S16) is not far from $q = 0$, the magnitude of the third term in RHS of Eq. (S20), which comes from the q^2-term of $\varepsilon(q)$, is small. To avoid the complicate solution of the cubic equation, instead, we treat the third term in RHS of Eq. (S20) as a small correction factor and approximate the $\varepsilon_{eff,S}$ in RHS of Eq. (S20) as the solution derived from the first-order approximation. (If one ignored the last term of Eq. (S20), the solution of the second-order approximation would just return to that of the first-order approximation.) Therefore, the solution of the second-order approximation is given by

$$\begin{aligned}\varepsilon_{eff,S} &\approx \varepsilon_{eff,S}^{(1)} + 2\left(\frac{e^2}{4\pi\varepsilon_0\hbar^2}\right)^2\frac{\mu_S^2 c_2}{\left(\varepsilon_{eff,S}^{(1)}\right)^2} \\ &= \frac{c_0}{2} + \frac{1}{2}\sqrt{c_0^2 + \frac{4e^2}{3\pi\varepsilon_0\hbar^2}\mu_S c_1} + 2\left(\frac{e^2}{4\pi\varepsilon_0\hbar^2}\right)^2\frac{\mu_S^2 c_2}{\left(\frac{c_0}{2} + \frac{1}{2}\sqrt{c_0^2 + \frac{4e^2}{3\pi\varepsilon_0\hbar^2}\mu_S c_1}\right)^2}.\end{aligned} \tag{S21}$$

Extended 2D-hydrogen model with the non-local dielectric screening

The energy splitting between the bright exciton (BX) and dark excitons (DX) is determined by

$$\Delta_{B,D}^{X} = \Delta_c + \Delta_{B,D}^{X(d)} + \Delta_{B,D}^{X(xc)}, \tag{S22}$$

where the conduction band splitting $\Delta_c = 19.6$ meV from the DFT calculation, $\Delta_{B,D}^{X(d)}$ is the direct-interaction-induced binding energy difference between BX and DX and $\Delta_{B,D}^{X(xc)}$ is the difference of the exchange energy between BX and DX. According to the discussion of the previous section, DX experiences the larger effective dielectric constant due to its heavier mass, i.e., $\varepsilon_{eff,D} = \varepsilon_{eff} + \Delta\varepsilon$, where $\varepsilon_{eff} \equiv \varepsilon_{eff,B}$. In the 2D-hydrogen model, the binding energy difference of BX and DX is given by

$$\begin{aligned}\Delta_{B,D}^{X(d)} &= E_D^b - E_B^b \\ &= 4Ry\left[\frac{\mu_D/m_0}{(\varepsilon_{eff}+\Delta\varepsilon)^2} + \frac{\mu_B/m_0}{\varepsilon_{eff}^2}\right] \\ &\approx 4Ry\left[\frac{\Delta\mu_{DB}/m_0}{\varepsilon_{eff}^2} - 2\Delta\varepsilon\frac{\mu_D/m_0}{\varepsilon_{eff}^3}\right],\end{aligned} \tag{S23}$$

where $\Delta\mu_{DB} = \mu_D - \mu_B$ is the difference of the reduced mass between BX and DX. In Eq. (S23), we take the first-order term of $\Delta\varepsilon$ to carry out the influence of the $\Delta\varepsilon$ on the BX-DX splitting.

The third term in Eq. (S26) is evaluated by $\Delta_{B,D}^{X} = V_B^x - V_D^x$, where V_S^x is the exchange energy of exciton state S. For the dipole-forbidden SFDX, $V_D^x = 0$ is vanishing. Hence, $\Delta_{B,D}^{X(xc)}$ is contributed solely from the exchange energy of BX. The exchange energy of an exciton state S is evaluated by

$$V_S^x = \frac{1}{\mathcal{A}}\sum_{vc\boldsymbol{k}}\sum_{v'c'\boldsymbol{k}'} A_{S,\boldsymbol{k}_{ex}}^{(0)*}(vc\boldsymbol{k})V_{\boldsymbol{k}_{ex}}^x(vc\boldsymbol{k}, v'c'\boldsymbol{k}')A_{S,\boldsymbol{k}_{ex}}^{(0)}(v'c'\boldsymbol{k}'), \tag{S24}$$

where $A_{S,\boldsymbol{k}_{ex}}^{(0)}(vc\boldsymbol{k})$ is the amplitude of the e-h configuration of the exchange-free exciton state, $V_{\boldsymbol{k}_{ex}}^x(vc\boldsymbol{k}, v'c'\boldsymbol{k}')$ is the kernel of the e-h exchange Coulomb interaction, and $\mathcal{A}$ is the area of TMD-ML. Similar to the way to evaluate the effective dielectric constant in Eq. (S16), we consider the exciton wavefunction $A_{S,\boldsymbol{k}_{ex}}^{(0)}(vc\boldsymbol{k})$ to be localized around the K or K' valley and simplified to be a constant as $|\boldsymbol{k} - \boldsymbol{K}| \leq 2/a_S^X$. Under the simplification, the difference of

exchange energies between BX and DX can be estimated by

$$\Delta_{B,D}^{X(xc)} \approx \frac{(\mu_B/m_0)^2}{\pi(a_0)^2}\frac{1}{\varepsilon_{eff}^2}\bar{v}^x(\boldsymbol{q}_0), \tag{S25}$$

where $a_0 = 0.53$ Å is the Bohr radius in the hydrogen atom, $\bar{v}^x(\boldsymbol{q}_0) \equiv \mathcal{A}V_{\boldsymbol{0}}^x(vc\boldsymbol{K}+\boldsymbol{q}_0, vc\boldsymbol{K}+\boldsymbol{q}_0)$ and $\boldsymbol{q}_0$ are the characteristic wave vectors for a BX with the magnitude $q_0 = 1/a_B^X$.

In Eq. (S23), the second term with $\Delta\varepsilon$ arises from the non-local dielectric screening and makes a negative ε_{eff}^{-3}-contribution to the BX-DX splitting. Thus, one can rewrite Eq. (S22) in terms of the parts respectively arising from the local and non-local screenings

$$\Delta_{B,D}^{X} = \Delta_{B,D}^{X(local)} + \Delta_{B,D}^{X(non-loc.)}, \tag{S26}$$

where the part contributed from the effective local screening is defined as

$$\Delta_{B,D}^{X(local)} = \Delta_c + 4\varepsilon_{eff}^{-2}\left[(\Delta\mu_{DB}/m_0)Ry + \frac{(\mu_B/m_0)^2}{4\pi(a_0)^2}\bar{v}^x(\boldsymbol{q}_0)\right], \tag{S27}$$

and the part contributed from the non-local screening is defined as

$$\Delta_{B,D}^{X(non-loc.)} = -8\varepsilon_{eff}^{-3}\Delta\varepsilon(\mu_D/m_0)Ry. \tag{S28}$$

Eqs. (S26) - (S28) constitute the extended exciton model with the consideration of non-local screening used for Fig.4 in the main article.

References

(1) Trolle, M. L.; Pedersen, T. G.; Véniard, V. Model dielectric function for 2D semiconductors including substrate screening. *Scientific reports* **2017**, *7*, 39844.

(2) Florian, M.; Hartmann, M.; Steinhoff, A.; Klein, J.; Holleitner, A. W.; Finley, J. J.; Wehling, T. O.; Kaniber, M.; Gies, C. The Dielectric Impact of Layer Distances on Exciton and Trion Binding Energies in van der Waals Heterostructures. *Nano Letters* **2018**, *18*, 2725–2732, PMID: 29558797.

(3) Kamban, H. C.; Pedersen, T. G.; Peres, N. M. R. Anisotropic Stark shift, field-induced dissociation, and electroabsorption of excitons in phosphorene. *Phys. Rev. B* **2020**, *102*, 115305.

(4) Kornyshev, A. A.; Rubinshtein, A. I.; Vorotyntsev, M. A. Model nonlocal electrostatics. I. *Journal of Physics C: Solid State Physics* **1978**, *11*, 3307.

(5) Peng, G.-H.; Lo, P.-Y.; Li, W.-H.; Huang, Y.-C.; Chen, Y.-H.; Lee, C.-H.; Yang, C.-K.; Cheng, S.-J. Distinctive Signatures of the Spin- and Momentum-Forbidden Dark Exciton States in the Photoluminescence of Strained WSe2 Monolayers under Thermalization. *Nano Letters* **2019**, *19*, 2299–2312, PMID: 30860847.

(6) Latini, S.; Olsen, T.; Thygesen, K. S. Excitons in van der Waals heterostructures: The important role of dielectric screening. *Phys. Rev. B* **2015**, *92*, 245123.

(7) Cappellini, G.; Del Sole, R.; Reining, L.; Bechstedt, F. Model dielectric function for semiconductors. *Phys. Rev. B* **1993**, *47*, 9892–9895.

(8) Katsch, F.; Selig, M.; Knorr, A. Exciton-Scattering-Induced Dephasing in Two-Dimensional Semiconductors. *Phys. Rev. Lett.* **2020**, *124*, 257402.

(9) Neamen, D. A. *Semiconductor physics and devices: basic principles*; McGraw-hill, 2012.

(10) Geick, R.; Perry, C. H.; Rupprecht, G. Normal Modes in Hexagonal Boron Nitride. *Phys. Rev.* **1966**, *146*, 543–547.

(11) Stier, A. V.; Wilson, N. P.; Velizhanin, K. A.; Kono, J.; Xu, X.; Crooker, S. A. Magnetooptics of Exciton Rydberg States in a Monolayer Semiconductor. *Phys. Rev. Lett.* **2018**, *120*, 057405.

(12) Birey, H. Thickness dependence of the dielectric constant and resistance of Al2O3 films. *Journal of Applied Physics* **1977**, *48*, 5209–5212.

(13) Peimyoo, N.; Barnes, M. D.; Mehew, J. D.; Sanctis, A. D.; Amit, I.; Escolar, J.; Anastasiou, K.; Rooney, A. P.; Haigh, S. J.; Russo, S.; Craciun, M. F.; Withers, F. Laser-writable high-k dielectric for van der Waals nanoelectronics. *Science Advances* **2019**, *5*, eaau0906.

(14) Kamban, H. C.; Pedersen, T. G.; Peres, N. M. R. Anisotropic Stark shift, field-induced dissociation, and electroabsorption of excitons in phosphorene. *Phys. Rev. B* **2020**, *102*, 115305.

(15) Van der Donck, M.; Peeters, F. M. Interlayer excitons in transition metal dichalcogenide heterostructures. *Phys. Rev. B* **2018**, *98*, 115104.

(16) Rasmussen, F. A.; Thygesen, K. S. Computational 2D materials database: electronic structure of transition-metal dichalcogenides and oxides. *The Journal of Physical Chemistry C* **2015**, *119*, 13169–13183.

(17) Pedersen, T. G.; Latini, S.; Thygesen, K. S.; Mera, H.; Nikolić, B. K. Exciton ionization in multilayer transition-metal dichalcogenides. *New Journal of Physics* **2016**, *18*, 073043.

(18) Kumar, A.; Ahluwalia, P. Tunable dielectric response of transition metals dichalco-

genides MX2 (M= Mo, W; X= S, Se, Te): Effect of quantum confinement. *Physica B: Condensed Matter* **2012**, *407*, 4627–4634.

(19) Chen, S.-Y.; Goldstein, T.; Taniguchi, T.; Watanabe, K.; Yan, J. Coulomb-bound four- and five-particle intervalley states in an atomically-thin semiconductor. *Nature Communications* **2018**, *9*, 3717.

(20) Kresse, G.; Furthmüller, J. Efficient iterative schemes for ab initio total-energy calculations using a plane-wave basis set. *Phys. Rev. B* **1996**, *54*, 11169–11186.

(21) Krukau, A. V.; Vydrov, O. A.; Izmaylov, A. F.; Scuseria, G. E. Influence of the exchange screening parameter on the performance of screened hybrid functionals. *The Journal of chemical physics* **2006**, *125*, 224106.

(22) Al-Hilli, A.; Evans, B. The preparation and properties of transition metal dichalcogenide single crystals. *Journal of Crystal Growth* **1972**, *15*, 93–101.

(23) Schutte, W.; De Boer, J.; Jellinek, F. Crystal structures of tungsten disulfide and diselenide. *Journal of Solid State Chemistry* **1987**, *70*, 207–209.

(24) Zhang, X.-X.; Cao, T.; Lu, Z.; Lin, Y.-C.; Zhang, F.; Wang, Y.; Li, Z.; Hone, J. C.; Robinson, J. A.; Smirnov, D., et al. Magnetic brightening and control of dark excitons in monolayer WSe 2. *Nature nanotechnology* **2017**, *12*, 883–888.

(25) Molas, M. R.; Faugeras, C.; Slobodeniuk, A. O.; Nogajewski, K.; Bartos, M.; Basko, D.; Potemski, M. Brightening of dark excitons in monolayers of semiconducting transition metal dichalcogenides. *2D Materials* **2017**, *4*, 021003.

(26) Zinkiewicz, M.; Grzeszczyk, M.; Kipczak, Ł.; Kazimierczuk, T.; Watanabe, K.; Taniguchi, T.; Kossacki, P.; Babiński, A.; Molas, M. R. The effect of dielectric environment on the brightening of neutral and charged dark excitons in WSe2 monolayer. *Applied Physics Letters* **2022**, *120*, 163101.

(27) Molas, M. R.; Slobodeniuk, A. O.; Kazimierczuk, T.; Nogajewski, K.; Bartos, M.; Kapuściński, P.; Oreszczuk, K.; Watanabe, K.; Taniguchi, T.; Faugeras, C.; Kossacki, P.; Basko, D. M.; Potemski, M. Probing and Manipulating Valley Coherence of Dark Excitons in Monolayer WSe_2. *Phys. Rev. Lett.* **2019**, *123*, 096803.

(28) Wang, G.; Robert, C.; Glazov, M. M.; Cadiz, F.; Courtade, E.; Amand, T.; Lagarde, D.; Taniguchi, T.; Watanabe, K.; Urbaszek, B.; Marie, X. In-Plane Propagation of Light in Transition Metal Dichalcogenide Monolayers: Optical Selection Rules. *Phys. Rev. Lett.* **2017**, *119*, 047401.

(29) Yang, M.; Ren, L.; Robert, C.; Van Tuan, D.; Lombez, L.; Urbaszek, B.; Marie, X.; Dery, H. Relaxation and darkening of excitonic complexes in electrostatically doped monolayer WSe_2: Roles of exciton-electron and trion-electron interactions. *Phys. Rev. B* **2022**, *105*, 085302.

(30) Robert, C.; Amand, T.; Cadiz, F.; Lagarde, D.; Courtade, E.; Manca, M.; Taniguchi, T.; Watanabe, K.; Urbaszek, B.; Marie, X. Fine structure and lifetime of dark excitons in transition metal dichalcogenide monolayers. *Phys. Rev. B* **2017**, *96*, 155423.

(31) Liu, E.; van Baren, J.; Liang, C.-T.; Taniguchi, T.; Watanabe, K.; Gabor, N. M.; Chang, Y.-C.; Lui, C. H. Multipath Optical Recombination of Intervalley Dark Excitons and Trions in Monolayer WSe_2. *Phys. Rev. Lett.* **2020**, *124*, 196802.

(32) Liu, E.; van Baren, J.; Lu, Z.; Altaiary, M. M.; Taniguchi, T.; Watanabe, K.; Smirnov, D.; Lui, C. H. Gate Tunable Dark Trions in Monolayer WSe_2. *Phys. Rev. Lett.* **2019**, *123*, 027401.

(33) Liu, E.; van Baren, J.; Taniguchi, T.; Watanabe, K.; Chang, Y.-C.; Lui, C. H. Valley-selective chiral phonon replicas of dark excitons and trions in monolayer WSe_2. *Phys. Rev. Res.* **2019**, *1*, 032007.

(34) Jadczak, J.; Glazov, M.; Kutrowska-Girzycka, J.; Schindler, J. J.; Debus, J.; Ho, C.-H.; Watanabe, K.; Taniguchi, T.; Bayer, M.; Bryja, L. Upconversion of Light into Bright Intravalley Excitons via Dark Intervalley Excitons in hBN-Encapsulated WSe2 Monolayers. *ACS Nano* **2021**, *15*, 19165–19174, PMID: 34735768.

(35) Zhou, Y.; Scuri, G.; Wild, D. S.; High, A. A.; Dibos, A.; Jauregui, L. A.; Shu, C.; De Greve, K.; Pistunova, K.; Joe, A. Y., et al. Probing dark excitons in atomically thin semiconductors via near-field coupling to surface plasmon polaritons. *Nature nanotechnology* **2017**, *12*, 856–860.

(36) He, M.; Rivera, P.; Van Tuan, D.; Wilson, N. P.; Yang, M.; Taniguchi, T.; Watanabe, K.; Yan, J.; Mandrus, D. G.; Yu, H.; Dery, H.; Yao, W.; Xu, X. Valley phonons and exciton complexes in a monolayer semiconductor. *Nature Communications* **2020**, *11*, 618.

(37) Ye, Z.; Waldecker, L.; Ma, E. Y.; Rhodes, D.; Antony, A.; Kim, B.; Zhang, X.-X.; Deng, M.; Jiang, Y.; Lu, Z.; Smirnov, D.; Watanabe, K.; Taniguchi, T.; Hone, J.; Heinz, T. F. Efficient generation of neutral and charged biexcitons in encapsulated WSe2 monolayers. *Nature Communications* **2018**, *9*, 3718.

(38) Barbone, M.; Montblanch, A. R.-P.; Kara, D. M.; Palacios-Berraquero, C.; Cadore, A. R.; De Fazio, D.; Pingault, B.; Mostaani, E.; Li, H.; Chen, B.; Watanabe, K.; Taniguchi, T.; Tongay, S.; Wang, G.; Ferrari, A. C.; Atatüre, M. Charge-tuneable biexciton complexes in monolayer WSe2. *Nature Communications* **2018**, *9*, 3721.

(39) Kapuściński, P.; Delhomme, A.; Vaclavkova, D.; Slobodeniuk, A. O.; Grzeszczyk, M.; Bartos, M.; Watanabe, K.; Taniguchi, T.; Faugeras, C.; Potemski, M. Rydberg series of dark excitons and the conduction band spin-orbit splitting in monolayer WSe2. *Communications Physics* **2021**, *4*, 186.

(40) Borghardt, S.; Tu, J.-S.; Taniguchi, T.; Watanabe, K.; Kardynał, B. E. Interplay of excitonic complexes in p-doped WSe_2 monolayers. *Phys. Rev. B* **2020**, *101*, 161402.

(41) Li, Z.; Wang, T.; Lu, Z.; Khatoniar, M.; Lian, Z.; Meng, Y.; Blei, M.; Taniguchi, T.; Watanabe, K.; McGill, S. A.; Tongay, S.; Menon, V. M.; Smirnov, D.; Shi, S.-F. Direct Observation of Gate-Tunable Dark Trions in Monolayer WSe2. *Nano Letters* **2019**, *19*, 6886–6893, PMID: 31487988.

(42) Li, Z.; Wang, T.; Lu, Z.; Jin, C.; Chen, Y.; Meng, Y.; Lian, Z.; Taniguchi, T.; Watanabe, K.; Zhang, S.; Smirnov, D.; Shi, S.-F. Revealing the biexciton and trion-exciton complexes in BN encapsulated WSe2. *Nature Communications* **2018**, *9*, 3719.

(43) Olsen, T.; Latini, S.; Rasmussen, F.; Thygesen, K. S. Simple Screened Hydrogen Model of Excitons in Two-Dimensional Materials. *Phys. Rev. Lett.* **2016**, *116*, 056401.